Supplementary Information

A Janus 3D DNA Nanomachine for Simultaneous and Sensitive Fluorescent Detection and Imaging of Dual MicroRNAs in Cancer Cells

Zezhou Yang, Xin Peng, Peng Yang, Ying Zhuo, Yaqin Chai, Wenbin Liang* and Ruo Yuan*

Key Laboratory of Luminescence Analysis and Molecular Sensing (Southwest University), Ministry of Education, College of Chemistry and Chemical Engineering, Southwest University, Chongqing 400715, PR China

Table of Contents

Chemical and Materials

Ethylenediaminetetraacetic acid (EDTA), Tris and $MgCl_2$ were acquired from Sigma Chemical Co. (St. Louis, MO, U.S.A.). Trisodium citrate dehydrate ($C_6H_5Na_3O_7 \cdot 2H_2O$) and trichloromethane ($CHCl_3$) was obtained from Chongqing Chuan Dong Chemical Co. (Chongqing, China). Tetraethoxysilane (TEOS) and hydrogen tetrachloroaurate (III) trihydrate ($HAuCl_4$) were purchased from Alfa Aesar Co., Inc. (Shanghai, China). 3-aminopropyl triethoxysilane (APTES) was provided by Aladdin Reagent Company (Shanghai, China). Ammonium hydroxide ($NH_3 \cdot H_2O$) (25-28%) was purchased from Chengdu Kelong Company Ltd. (Chengdu, China). N-(3-dimethylaminopropyl)-N′-ethylcarbodiimide hydrochloride (EDC) and N-hydroxy succinimide (NHS) were obtained from Shanghai Medpep Co. (Shanghai, China). Paraffin wax (T_m: 52-54 °C) was purchased from Sinopharm Chemical Reagent Co., Ltd. Tris-(2-carboxyethyl)-phosphine hydrochloride (TCEP) was bought from Sangon Biotech Co., Ltd. (Shanghai, China). Gel green nucleic acid dye was obtained from Genview Scientific Inc. (Shanghai, China) for gel imaging. TE buffer (pH 8.0) was made up of 10 mM Tris-HCl, 1 mM EDTA and 15 mM $MgCl_2$ standard stock solutions. Dulbecco's Modified Eagle Medium (DMEM), phosphate buffered saline (PBS) and 4% paraformaldehyde were provided by Thermo Fisher Scientific Inc. (Shanghai, China) for cell experiment. All the other chemicals were analytical grade and used without further purification. The deionized water was purified by a water purification system with the electrical resistance of 18.2 MΩ/cm.

The oligonucleotides (**Table S1**) employed in this work were custom-synthesized

by Shanghai Sangon Biological Engineering Technology and Services Company, Ltd. (Shanghai, China). Before using, the hairpin nucleotides (H1, H2, H3, H4, H6, H7, H9, H10, H11 and H12) were heated to 95 °C for 5 min and then progressively cooled down to room temperature to form stem-loop structure.

Table S1. Oligonucleotide sequences information used in the experiments

Names	Sequences (5'-3')
miRNA-21	UAG CUU AUC AGA CUG AUG UUG A
miRNA-155	UUA AUG CUA AUC GUG AUA GGG GU
H1	SH-CAA TTC TTC AGG TCA ACA AGT AGT ATG TAA TGT GTG TAG ATG TTG ACC TG-FAM
H2	COOH-TTT TTT TTT TAC AAA ACA GTA CCC CTA TAA AGT GAT CCC GGT ATG CAT TTA GGG GTA CTG T
H3	AGA CTG ATG TTG ACC TGA AGA ATT GTG AGA TCT CAA CAT CAG TCT GAT AAG CTA
H4	TGT TGA CCT GAA GAA TTG TGA GAT CTC GTG TTT ATA GGA TGT TGA CCT GAA GAA TTG TAG CTT ATC AGA CTG ATG TTG AGA TCT CAC AAT TCT TCA GGT CAA CAT CAG TCT
H5	CAA TTC TTC AGG TCA ACA TCC TAT AAA CAC GAG ATC TCA CAA TTC TTC AGG TCA ACA
A	TGT TGA CCT GAA GAA TTG CTT ATC ACT ACC AAA CGA ATA TGT TGA CCT GAA GAA TTG
H6	ATC GTG ATA GGG GTA CCG TTT TGT ATA ACT CAC ACC CCT ATC ACG ATT AGC ATT AA
H7	TAG GGG TAC TGT TTT GTA TAA CTC CGT CTG GGT TTA CTC TAG GGG TAC TGT TTT GTA TTA ATG CTA ATC GTG ATA GGG GTG TGA GTT ATA CAA AAC GGT ACC CCT ATC ACG AT
H8	TAC AAA ACA GTA CCC CTA GAG TAA ACC CAG ACG GAG TTA TAC AAA ACA GTA CCC CTA
B	TAG GGG TAC TGT TTT GTA ATT TAA GGA AGA TTC GGT GTT TAG GGG TAC TGT TTT GTA
H9	GGT CAA CAT CTA CAC ACA TTA CAT ACT ACT TGT TGA CCT GAA GAA TTG TGT GTG TAG ATG
H10	Cy5-AGT ACC CCT AAA TGC ATA CCG GGA TCA CTT TAT AGG

	GGT ACT GTT TTG TAC GGT ATG CAT TTA GG-BHQ
H11	SH-TTT ACA AAA CAG TAC CCC TAT AAA GTG ATC CCG GTA TGC ATT TAG GGG TAC TGT- Cy5
H12	AGT ACC CCT AAA TGC ATA CCG GGA TCA CTT TAT AGG GGT ACT GTT TTG TAC GGT ATG CAT TTA GG
FAM-FISH	FAM-TCA ACA TCA GTC TGA TAA GCT A
C	AGA CTG ATG TTG A-BHQ
Cy5-FISH	Cy5-ACC CCT ATC ACG ATT AGC ATT AA
D	TCG AGA TAG GGG T-BHQ
miRNA-122	UGG AGU GUG ACA AUG GUG UUU G
miRNA-126	CAU UAU UAC UUU UGG UAC
miRNA-141	UAA CAC UGU CUG GUA AAG AUG G
miRNA-203a	AGU GGU UCU UAA CAG UUC AAC AGU U
miRNA-182-5P	UUU GGC AAU GGU AGA ACU CAC ACU

Apparatus

The fluorescence signal responses were carried out on an F-7000 fluorescence spectrophotometer (Hitachi, Tokyo, Japan) with 5 nm slit widths of both excitation and emission and the PMT voltage of 950 V in all fluorescent experiments. Native polyacrylamide gel electrophoresis was performed with a BG-verMIDI standard vertical electrophoresis apparatus (Baygene, China) and a Gel Doc XR$^+$ System (Bio-Rad, California, U.S.A.). Confocal fluorescence imaging was operated on confocal laser scanning microscope 900 (Zeiss LSM 900, Germany) with an objective lens (64 ×). The morphologies and sizes of the nanomaterials were characterized by scanning electron microscope (SEM, FEI Nova NanoSEM450). Ultraviolet-visible (UV-vis) absorption spectrums were accomplished with UV-2450 UV-vis spectrophotometer

(Shimadzu, Tokyo, Japan). The Zeta potential was performed by Malvern ZEN3690 (Malvern Panalytical, England). A PHS-3C digital pH-meter (Shanghai LeiCi Device Works, Shanghai, China) was employed to test the pH of all solutions in the whole experiments.

Preparation of Amino-Modified SiO_2 Nanoparticles (SiO_2-NH_2 NPs)

SiO_2-NH_2 NPs of 300 nm size were synthesized using a multistep hydrolysis-condensation procedure of TEOS in ammonia hydroxide-ethanol solution based on the Stöber approach.[1] Briefly, 2 mL of TEOS was dispersed in 16.5 mL of ethanol with stirring for 20 min. Simultaneously, 2 mL of $NH_3 \cdot H_2O$, 16.5 mL of ethanol and 6 mL of deionized water were mixed and stirred for 20 min to get homogeneous solution. Next, the two mixture solution were added to a flask and the final solution was stirred in a water bath at 30 ºC for 15 h. Then, the mixture was centrifugally washed with ethanol for five times and the obtained SiO_2 NPs were resuspended in ethanol. Subsequently, 0.5 mL of amino reagent APTES was added in 30 mL of SiO_2 NPs ethanol solution. Then, this mixture was vigorously stirred and heated to 76 °C under refluxing for over 24 h. The obtained SiO_2-NH_2 NPs were purified by centrifugation with ethanol for five times. After washing, the SiO_2-NH_2 NPs were resuspended in deionized water and stored at 4 °C for the subsequent use.

Preparation of Au@SiO_2 NPs

Au NPs with a diameter of 16 nm were synthetized by the reduction of $HAuCl_4$ in

aqueous solution according to the previous work.[2] In brief, 1.0 mL of trisodium citrate aqueous solution (1% *w*/*V*) was added to 50 mL of boiling and vigorously stirred $HAuCl_4$ solution (0.01% *w*/*V*) to keep boiling with a stirring for 15 min, and then naturally cooled to room temperature. Next, the resultant colloidal suspension (Au NPs) was centrifugally washed with deionized water for three times and the obtained Au NPs were redispersed in deionized water. 10 μL of SiO_2-NH_2 NPs and 15 mL of Au NPs were mixed and then stirred at room temperature for 16 h with a homogenizer at a speed of 500 rpm. Shortly after, the mixture was centrifugally washed with deionized water for three times to collect the Au@SiO_2 NPs. The Au NPs was covalently attached to the surface of SiO_2-NH_2 NPs *via* Au-N bonds. The obtained Au@SiO_2 NPs solution was stored in the dark at 4 °C for the further use.

Preparation of Janus Nanoparticles

The preparation process of the Janus nanoparticles was shown in **Fig. S1**. A mixture of 100 μL SiO_2-NH_2 NPs, 150 μL HCl (2 M) solution, and 1 g paraffin wax was added to 10 mL of water. The mixture was emulsified at 80 °C with a homogenizer at a speed of 800 rpm for 1 h to form a wax-in-water emulsion and then was cooled to room temperature, at which paraffin wax was solid. Afterwards, the wax emulsions was washed with deionized water for three times to remove particles in the aqueous solution as well as weakly attached and unattached SiO_2-NH_2 NPs. The resulting exposed surfaces of SiO_2-NH_2 NPs attached to the emulsions were mixed with 10 mL Au NPs and stirred at room temperature for 16 h, leading the Au NPs covalently attached to the

surface of SiO_2-NH_2 NPs *via* Au-N bonds. After that, the reaction solutions were washed with deionized water for multiple times to remove weakly attached and unattached Au NPs. Finally, in order to release these Janus nanoparticles from wax, the wax was dissolved in $CHCl_3$ at room temperature and collected by centrifugation. The obtained Janus nanoparticles were resuspended in deionized water and stored in the dark at 4 °C for the subsequent use.

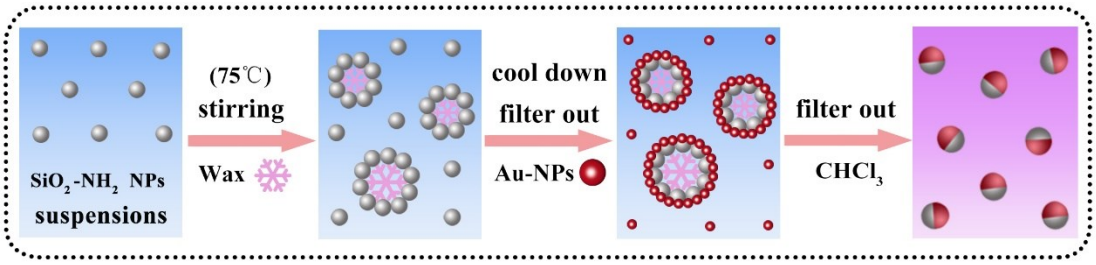

Fig. S1. Schematic representation of the preparation process of Janus nanoparticles.

Preparation of Janus 3D DNA Nanostructure

The Janus nanoparticles were functionalized with oligonucleotides through the literature procedures with minor modification.[3,4] Briefly, 50 μL of the thiolated oligonucleotide solution H1 (4 μM) was mixed with 5 μL of TCEP (20 mM) at 37 °C for 1 h to reduce residual disulfide bonds, where H1 labeled with FAM as fluorescence indicator. After that, 50 μL of the carboxyl-modified oligonucleotide solution H2 (4 μM) was mixed with 5 μL of a mixture of EDC and NHS (4:1) at 37 °C for 1 h to activate the carboxyl. Next, 30 μL H1 and 30 μL H2 were mixed with the solution of 20 μL Janus nanoparticles, followed by incubated at 37 °C for 5 h to obtain DNA-functionalized Janus nanoparticles suspension solution. Finally, unattached thiolated

oligonucleotide H1 and carboxylated oligonucleotide H2 was thoroughly removed by centrifugation for 15 min at 4 °C and washed twice with TE buffer. The Janus 3D DNA nanostructure was assembled by anchoring FAM and sulfydryl-labeled H1 and carboxyl-labeled H2 on the two different hemispheres of Janus nanoparticles *via* Au-S and CO-NH bonds interaction, respectively. After washing, the Janus 3D DNA nanostructure were resuspended in 40 μL TE buffer and stored at -20 °C for the subsequent use.

Target Recycling and Fluorescent Measurements

The different concentrations of miRNA-21 (1 pM, 5 pM, 10 pM, 50 pM, 100 pM, 500 pM, 1 nM, 5 nM and 10 nM), H3 (2 μM), H4 (2 μM) and A-H5 hybrids were mixed and incubated at 37 °C for 2 h to achieve target recycling, which could produce numerous exposed sticky ends of H3-H4 hybrids to hybridize with H5 on A-H5 hybrids to export double feet catalyst strands A. At the same time, the various concentrations of miRNA-155 (1 pM, 5 pM, 10 pM, 50 pM, 100 pM, 500 pM, 1 nM, 5 nM, and 10 nM), H6 (2 μM), H7 (2 μM) and B-H8 hybrids were mixed and incubated at 37 °C for 2 h to achieve target recycling, which could export a large number of exposed sticky ends of H6-H7 hybrids to hybridize with H8 on B-H8 hybrids to release double feet catalyst strands B. Subsequently, DNA-functionalized Janus nanoparticles solution were added to the target recycling reaction system to initiate the DNA walker amplification. With the addition of H9 (2 μM) and H10 (2 μM), the detection system was incubated at 37 °C for 40 min. Fluorescent data was collected from 510 nm to 750

nm on excitation of 497 nm and 640 nm. The max fluorescence emission at 520 nm and 665 nm were employed as the indicator to estimate the capability of the miRNA-21 and miRNA-155 detection approach, respectively.

Native Polyacrylamide Gel Electrophoresis (PAGE)

Firstly, 10 μL of each sample was mixed with 2 μL of 6 × loading buffer. And then, 10 μL of mixture was transferred into the native polyacrylamide gel (16%), respectively. Electrophoresis was performed in 1 × TBE (pH 8.0) at a 120 V constant voltage for 90 min. Subsequently, the gels were stained with Gel Red for 10 min and then transferred to Gel Doc XR^+ System for gel imaging to obtain the electrophoresis results.

Cell Culture and Cell Lysate Preparation

Human breast cancer cells (MCF-7 cells) and human cervical cancer cells (HeLa cells) were selected to perform the practical tests. HeLa and MCF-7 cells were cultured in DMEM medium containing 1% non-essential amino acids, 100 U/mL penicillin and 10% fetal bovine serum (FBS) at 37 °C with a humidified atmosphere (95% air and 5% CO_2). After 24 h cultivation, 10^6 cells were collected in the exponential phase and washed twice with sterile PBS. The total RNA extraction for the real sample detection was obtained using the Trizol Reagent Kit (Sangon, Inc., Shanghai, China) according to the manufacturer's protocol. Finally, the obtained cellular extracts were diluted and stored at -20 °C for further use.

Confocal Fluorescence Imaging of miRNAs by the Different 3D DNA Nanostructures

Human breast cancer cells MCF-7 (MCF-7 cells) and human cervical cancer cells HeLa (HeLa cells) were introduced into a 35 mm^2 Petri dish. Immediately, they were respectively cultured in DMEM medium with a humidified atmosphere (5% CO_2) at 37 °C for 24 h to reach 80% cell anchorage-dependent rate, and then washed with sterile PBS. Next, H1 modified Au@SiO_2-NH_2 NPs, H2 modified SiO_2-NH_2 NPs and H1/H2 modified Janus nanoparticles were mixed with corresponding DNA substrates. After that, the 50 μL of mixture was separately added into MCF-7 cells Petri dish and HeLa cells Petri dish to incubate 4 h. The cells were then stained with a Hoechst 33342 solution for 10 min and washed three times with 1× PBS. After washing, the cells were incubated with 1 mL of fresh DMEM medium at 37 °C before confocal fluorescence imaging.

Confocal Fluorescence Imaging of miRNAs by FISH

MCF-7 Cells and HeLa cells were seeded on confocal laser culture dishes and maintained in an air humidity of 5% CO_2 at 37°C. They were respectively cultured in DMEM medium with a humidified atmosphere (5% CO_2) at 37 °C for 24 h to reach 80% cell anchorage-dependent rate, and then washed with sterile PBS. For the detection of miRNAs by FISH approach, the FAM-labeled FISH probes hybridized with BHQ-labeled C and the Cy5-labeled FISH probes hybridized with BHQ-labeled D to generate

signal duplexes. And then, the 50 μL of FAM/BHQ-labeled MBs and Cy5/BHQ-labeled MBs solution was separately added into MCF-7 cells Petri dish and HeLa cells Petri dish to incubate 4 h, resulting in releasing BHQ-labeled C and BHQ-labeled D. The cells were then stained with a Hoechst 33342 solution for 10 min and washed three times with 1× PBS. After washing, the cells were incubated with 1 mL of fresh DMEM medium at 37 °C before confocal fluorescence imaging.

PAGE Characterization of the Proposed Biosensor

PAGE was employed to demonstrate the reaction mechanism of the proposed nonenzymatic Janus 3D DNA nanomachine based on cascade signal amplification strategy. The detection process of target miRNA-21 was shown in **Fig. S2A**. A bright single band could be clearly observed in lane c with lower mobility, suggesting that the target recycling was triggered to generate the hybrids between target miRNA-21 (lane a) and H3 (lane b). The stable formation of the H3 with H4 in lane e, which was authenticated by the band with mobility lower than H3 in lane b and H4 in lane d. Lane f and lane g represented double feet catalyst strands A and H5, respectively. Lane h represented the A/H5 hybrids. Four clear bands can be observed in lane i, and the top band represented H3/H4/H5 hybrids. The middle bands represented H3/H4 hybrids, A/H5 hybrids and double feet catalyst strands A. Lane j and lane m represented H1 and H9, respectively. Lane k consisted of two clear bands. The lower band was the H1/A/H1 hybrids and the higher one was H3/H4/H5 hybrids, which proved that the H3/H4 hybrids could hybridize with H5 on A/H5 hybrids to release the double feet catalyst

strands A to initiate Janus 3D DNA nanomachine. Three distinct bands could be clearly observed in lane n, and the top band represented H3/H4/H5 hybrids. The middle band represented H1/H9 hybrids and the bottom band represented double feet catalyst strands A, which indicated that the formation of the H1/H9 signal duplex labeled with fluorophore FAM and the release of double feet catalyst strands A for next recycle. Lane n and lane o revealed the PAGE results for the proposed Janus 3D DNA nanostructure in the presence of and in the absence of miRNA-21, respectively. As expected, H1/H9 signal duplex labeled with fluorophore FAM, H3/H4/H5 hybrids and the double feet catalyst strands A were obviously observed in comparison with lane o, which demonstrated the miRNA-21 could trigger the CHA DNA amplification to produce massive double feet catalyst stands A to efficiently walk on the surface of one hemispheres of Janus nanoparticles to generate numerous FAM-labeled duplexes for sensitive detection of target miRNA-21.

The detection process of target miRNA-155 was shown in **Fig. S2B**. A bright single band could be obviously observed in lane 3 with lower mobility, indicating that the target recycling was triggered to generate the hybrids between target miRNA-155 (lane 1) and H6 (lane 2). Lane 5 showed the PAGE results for the hybridization of H6 with H7, which was confirmed by the band with mobility lower than the H6 in lane 2 and H7 in lane 4. Lane 6 and lane 7 represented double feet catalyst strands B and H8 and exhibited a distinct single band, respectively. Lane 8 represented the B/H8 hybrids. In lane 9, four clear bands could be observed, and the top band presented the H6/H7/H8 hybrids. The other bands represented H6/H7 hybrids, B/H8 hybrids and double feet

catalyst strands B, suggesting that the exposed sticky ends of H6/H7 hybrids to hybridize with H8 on B/H8 hybrids to release the double feet catalyst strands B. H2 and H10 exhibited a distinct single band in lanes 10 and 12, respectively. In the lane 11, the band of H2/B/H2 hybrids were obviously observed in comparison with lane 10, which demonstrated the double feet catalyst strands B could initiate Janus 3D DNA nanomachine by hybridization with H2. Lanes 13 and 14 displayed the PAGE results for the proposed 3D DNA nanomachine in the presence of and in the absence of miRNA-155, respectively. As expected, no obvious band of the H2/H10 signal duplex labeled with fluorophore Cy5 and released double feet catalyst strands B were observed in lane 14. On the contrary, these two bright bands in lane 13 under the band of H6/H7/H8 hybrids could be obviously observed, indicating that the target-recycling was not triggered to initiate Janus 3D DNA nanomachine in the absence of target miRNA-155. Comparing the results of lane 13 to lane 14, the distinction sufficiently verified the specific response to the target miRNA-155 of the proposed strategy.

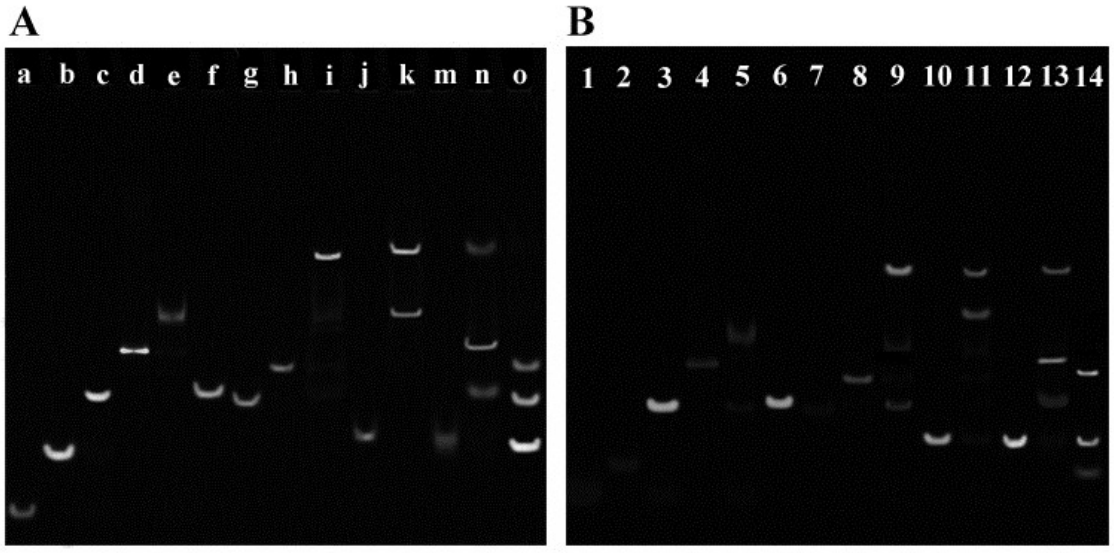

Fig. S2. (A) Characterization of the proposed dual-color 3D DNA Janus nanomachine for detection

of miRNA-21 by PAGE. Lane a: miRNA-21; lane b: H3; lane c: miRNA-21 with H3; lane d: H4; lane e: H3 with H4; lane f: A; lane g: H5; lane h: A with H5; lane i: H3, H4 and H5; lane j: H1; lane k: A and H1; lane m: H9; lane n: H1 and H9; lane o: without miRNA-21. (B) Native 16% PAGE analysis of our dual-color 3D DNA Janus nanomachine for detection of miRNA-155. Lane 1: miRNA-155; lane 2: H6; lane 3: miRNA-155 with H6; lane 4: H7; lane 5: H6 with H7; lane 6: B; lane 7: H8; lane 8: B with H8; lane 9: H6, H7 and H8; lane 10: H2; lane 11: B and H2; lane 12: H10; lane 13: H2 and H10; lane 14: without miRNA-155.

The PAGE analysis was further performed to make sure that no self-reaction occurred between H3 and H4, H6 and H7, and the two CHA reactions could work simultaneously without interfering with each other. As shown in **Fig. S3A**, a bright single band could be clearly observed in lane 3 with lower mobility, suggesting that the target recycling was triggered to generate the hybrids between H3 (lane 1) and H4 (lane 2). Two distinct bands could be clearly observed in lane 4, and the bottom and the top band respectively represented H3 and H4, which indicated that no self-reaction occurred between H3 and H4 in the absence of miRNA-21. In the lane 5, three clear bands could be observed, and the top band represented H4. The middle and the bottom bands respectively represented H3 and miRNA-155, which suggested that H3 and H4 hybridization reaction could be triggered only in the presence of miRNA-21. As shown in **Fig. S3B**, a bright single band could be obviously observed in lane III with lower mobility, indicating that the target recycling was triggered to generate the hybrids between H6 (lane I) and H7 (lane II). Two distinct bands could be clearly observed in lane IV, and the bottom and the top band respectively represented H6 and H7, which

demonstrated that no self-reaction occurred between H6 and H7 in the absence of miRNA-155. In the lane V, three clear bands could be observed, and the top band represented H7. The middle and the bottom bands respectively represented H6 and miRNA-21. As expected, H6/H7 hybrids could not be observed in comparison with lane III, which suggested that H6 and H7 hybridization reaction could be triggered only in the presence of miRNA-155. In order to characterize the proposed two CHA reactions without interfere with each other for simultaneous detection of target miRNA-21 and miRNA-155, the PAGE was further performed in **Fig. S3C**. Lane a, lane b, lane c and lane d represented H3, H4, H6 and H7, respectively. Three distinct bands could be clearly observed in lane e. However, no H3/H4 and H6/H7 hybrids were observed in lane e, which demonstrated that no self-reaction occurred between H3/H4 and H6/H7 in the absence of miRNA-21 and miRNA-155. In the lane f, four clear bands could be observed, and the top band represented H3/H4 hybrids. The other bands represented H6, H7 and miRNA-21, respectively. In the lane g, the top band represented H6/H7 hybrids and the other bands represented H3, H4 and miRNA-155, respectively. As expected, H3/H4 and H6/H7 hybrids could be observed at the top of lane h and no other unrelated bands were generated. These results demonstrated that the two CHA reactions could work simultaneously and did not interfere with each other for detection of target miRNA-21 and miRNA-155.

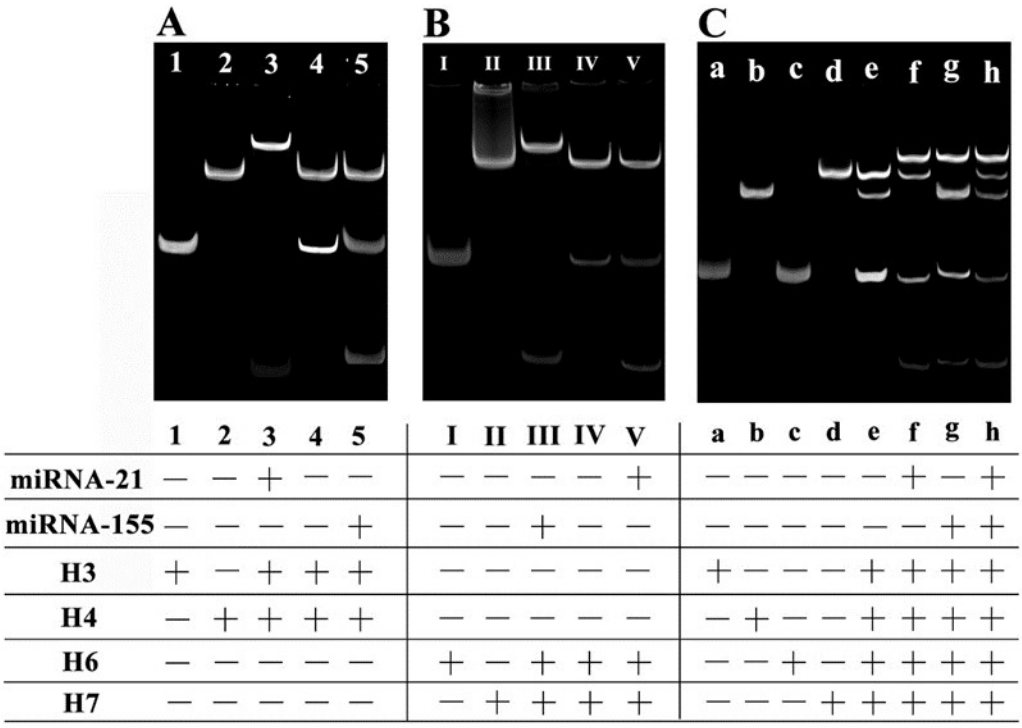

	1	2	3	4	5	I	II	III	IV	V	a	b	c	d	e	f	g	h
miRNA-21	−	−	+	−	−	−	−	−	−	+	−	−	−	−	−	+	−	+
miRNA-155	−	−	−	−	+	−	−	+	−	−	−	−	−	−	−	−	+	+
H3	+	−	+	+	+	−	−	−	−	−	+	−	−	−	+	+	+	+
H4	−	+	+	+	+	−	−	−	−	−	−	+	−	−	+	+	+	+
H6	−	−	−	−	−	+	−	+	+	+	−	−	+	−	+	+	+	+
H7	−	−	−	−	−	−	+	+	+	+	−	−	−	+	+	+	+	+

Fig. S3. (A) Characterization of self-reaction between H3 and H4. Lane 1: H3; lane 2: H4; lane 3: miRNA-21, H3 and H4; lane 4: H3 and H4; lane 5: miRNA-155, H3 and H4. (B) Characterization of self-reaction between H6 and H7. Lane I: H6; lane II: H7; lane III: miRNA-155, H6 and H7; lane IV: H6 and H7; lane V: miRNA-21, H6 and H7. (C) Characterization of the proposed two CHA reactions without interfere with each other for simultaneous detection of target miRNA-21 and miRNA-155. Lane a: H3; lane b: H4; lane c: H6; lane d: H7; lane e: H3, H4, H6 and H7; lane f: miRNA-21, H3, H4, H6 and H7; lane g: miRNA-155, H3, H4, H6 and H7; lane h: miRNA-21, H3, H4, miRNA-155, H6 and H7.

The Stability Study of the Janus Nanoparticle

In order to prove the stability of Janus nanoparticle, we have performed some extra experiments. Firstly, the carboxyl-labeled H2 and FAM and sulfydryl-labeled H1 were respectively immobilized on the two different hemispheres of Janus nanoparticles

composed of amino group (-NH_2) and Au NPs *via* CO-NH and Au-S bonds. If the DNA-functionalized Janus nanoparticles were unstable, the FAM would keep away from the Au NPs or even separate from the Janus nanoparticles over a long period of time, leading to fluorescence enhancement of the FAM. As shown in **Fig. S4A**, the DNA-functionalized Janus nanoparticles suspension solution observed low fluorescence signal of the FAM. With the increase of the storage time, the fluorescence intensity of FAM was approximately consistent, suggesting that the DNA-functionalized Janus nanoparticles were stable for the proposed fluorescent assay. Next, in order to further demonstrate the stability of dual-color Janus nanoparticles, the target recycling reaction system and H9 and H10 were added to DNA-functionalized Janus nanoparticles solution, and then the detection system was incubated at 37 °C for 40 min to keep the FAM and Cy5 away from Au NPs and quenchers BHQ respectively, resulting in recovery of two remarkable fluorescence. As shown in **Fig. S4B**, dual-color Janus nanoparticles suspension solution obtained two strong fluorescence of FAM and Cy5. Moreover, with the increase of the storage time, the fluorescence signal intensity of FAM and Cy5 was approximately consistent, indicating that dual-color Janus nanoparticles were stable for the simultaneous fluorescent detection of miRNA-21 and miRNA-155.

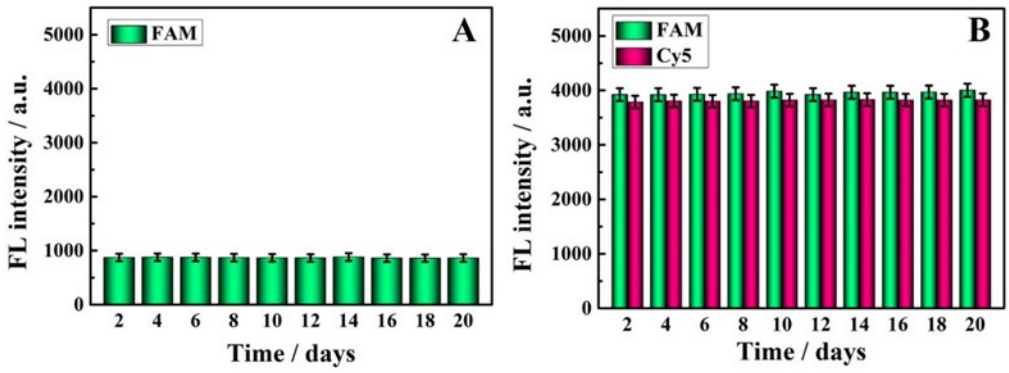

Fig. S4. (A) The stability of DNA-functionalized Janus nanoparticles from one to twenty days. (B) The stability of DNA-functionalized Janus nanoparticles in the presence of corresponding DNA substrates and miRNA-21 and miRNA-155 with 1nM from one to twenty days.

The Cytotoxicity Study of the Janus Nanoparticle

The cytotoxicity of the synthesized Janus nanoparticles was evaluated based on the MTT assay with HeLa cells. Firstly, the cells (1.0×10^5 cells per well) were seeded in 96-well microliter plates and cultured for 24 h in a humid atmosphere with 5% CO_2 at 37 °C. After rinsed by PBS, 10 μL of Janus nanoparticle with different dilutions and 90 μL of DMEM were added to incubate at 37 °C for 24 h. After washing with DMEM, 20 μL of MTT solution (5 mg/mL) with 80 μL of DMEM were added to incubate at 37 °C for 4 h. Finally, after removing the medium with MTT carefully, 100 μL dimethylsulfoxide (DMSO) was added to each well to dissolve the precipitates, followed by swayed with 15 min, which was evaluated by Multiskan Spectrum microplate reader at 570 nm. As shown in **Fig. S5**, as comparison with Au nanoparticles, the synthesized Janus nanoparticle performed a favored biocompatibility with a relatively low cytotoxic, which could be employed in the simultaneous and sensitive fluorescent imaging of miRNA-21 and miRNA-155 in cancer cells.

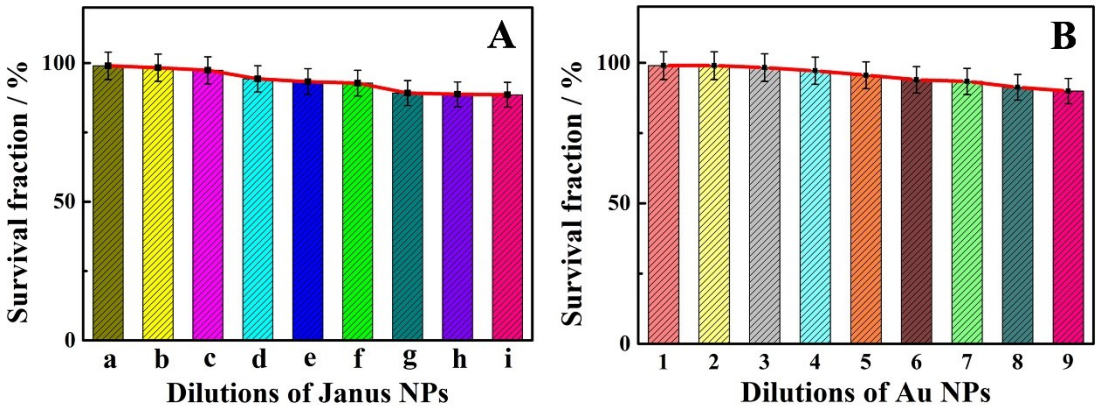

Fig. S5. (A) MTT assay for testing the cytotoxic of the synthesized Janus nanoparticles, (a) 1:1000; (b) 1:500; (c) 1:100; (d) 1:50; (e) 1:25; (f) 1:10; (g) 1:5; (h) 1:2.5; (i) 1:1. (B) MTT assay for testing the Au nanoparticles as control, (1) 1:1000; (2) 1:500; (3) 1:100; (4) 1:50; (5) 1:25; (6) 1:10; (7) 1:5; (8) 1:2.5; (9) 1:1.

Feasibility of the Proposed Strategy

In order to verify the feasibility of our proposed fluorescent assay for miRNA-21 and miRNA-155, a series of *in vitro* experiments were performed. As shown in **Fig. S6A**, without the target miRNA-21, a low fluorescence signal could be observed (**Fig. S6A**, curve a). In the presence of miRNA-21 but without H3 or H4, it hardly induced signal changes (**Fig. S6A**, curves b and c), indicating that without H3 or H4, target recycling could not be triggered to export massive H3/H4 hybrids for hybridization with H5 on A/H5 hybrids to release the double feet catalyst strands A. In the absence of A/H5 hybrids and H9, the test solution could also present a weak fluorescence signal (**Fig. S6A**, curves d and e). On the countrary, in the presence of 500 pM target miRNA-21, a significantly amplified fluorescence signal could be observed (**Fig. S6A**, curve f). When the target miRNA-21 was added, the target recycling was triggered to generate

multiple H3/H4 hybrids with an exposed sticky end for hybridization with H5 on A/H5 hybrids to release the double feet catalyst strands A, resulting in unlocking 3D DNA walker. The exposed sticky end of H1 could hybridize with H9 and release the double feet catalyst strands A for moving along with the 3D DNA tracks, leading to the fluorophore FAM kept away from the surface of the Au NPs and realize the remarkable fluorescence enhancement of FAM. As shown in **Fig. S6B**, without miRNA-155, H6, H7 and B/H8 hybrids exhibited a low fluorescence intensity (**Fig. S6B**, curves a, b, c and d). As expected, in the presence of 500 pM target miRNA-155, a relatively strong fluorescence signal could be observed (**Fig. S6B**, curve e). These results proved that our proposed Janus 3D DNA nanomachine was feasible for fluorescence detection of miRNA-21 and miRNA-155.

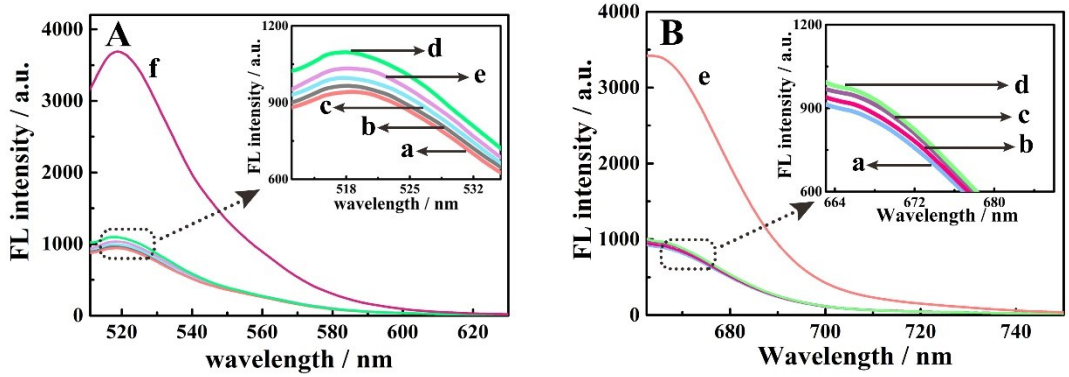

Fig. S6. (A) Fluorescence emission spectra with different experiment conditions of the proposed fluorescent strategy on the excitation of 497 nm for the detection of miRNA-21. (a) without miRNA-21, (b) without H3, (c) without H4, (d) without A/H5 hybrids, (e) without H9, (f) with miRNA-21. (B) Fluorescence emission spectra with different experiment conditions of the proposed fluorescent strategy on the excitation of 640 nm for the detection of miRNA-155. (a) without miRNA-155, (b) without H6, (c) without H7, (d) without B/H8 hybrids, (e) with miRNA-155.

Optimization of the Experimental Conditions

The experimental parameters could affect the detection efficiency and performance of the proposed fluorescent assay. Herein, a range of significant influencing factors were optimized based on the fluorescent determination of miRNA-21 and miRNA-155, including the concentration of H1 and H2, the incubation time of the miRNA-21 and miRNA-155 for exporting A and B, Fluorescence recovery time of the fluorophore FAM and Cy5.

The concentration of H1 and H2 was an extremely momentous factor for the detection efficiency and imaging performance of the proposed strategy. The fluorescent response at different concentrations of H1 and H2 were investigated from 1 to 6 μM (**Fig. S7A and S7B**). The fluorescent signal intensity reached a peak when the concentration of H1 and H2 was 4 μM, indicating the optimum performance for the detection of miRNA-21 and miRNA-155.

To investigate the effect of the incubation time of the miRNA-21 and miRNA-155 for exporting A and B, the proposed fluorescent assay was used for the detection of miRNA-21 and miRNA-155 with incubation time from 0.5 to 3 h. As shown in **Fig. S7C and S7D**, the relationship between the incubation time and the fluorescent signal response was studied. The fluorescent signal expeditiously increased with incubation time and then trended to a constant value after 2 h. Therefore, a topgallant incubation time of 2 h was employed for the consecutive fluorescent assays in this study.

Fluorescence recovery time of the fluorophore FAM and Cy5 was the key factor,

which could influence the fluorescent signal intensity of the FAM and Cy5 and significantly reduce sensitivity of fluorescent imaging. Therefore, the different fluorescence recovery time of the fluorophore FAM and Cy5 was investigated as shown in **Fig. S7E and S7F**. The experiment results indicated that the fluorescent intensity increased rapidly with gradually increasing the reaction time and reached the maximum at 40 min. Thus, the reaction time of fluorophore FAM and Cy5 of 40 min was used as optimal incubation time for all subsequent assays.

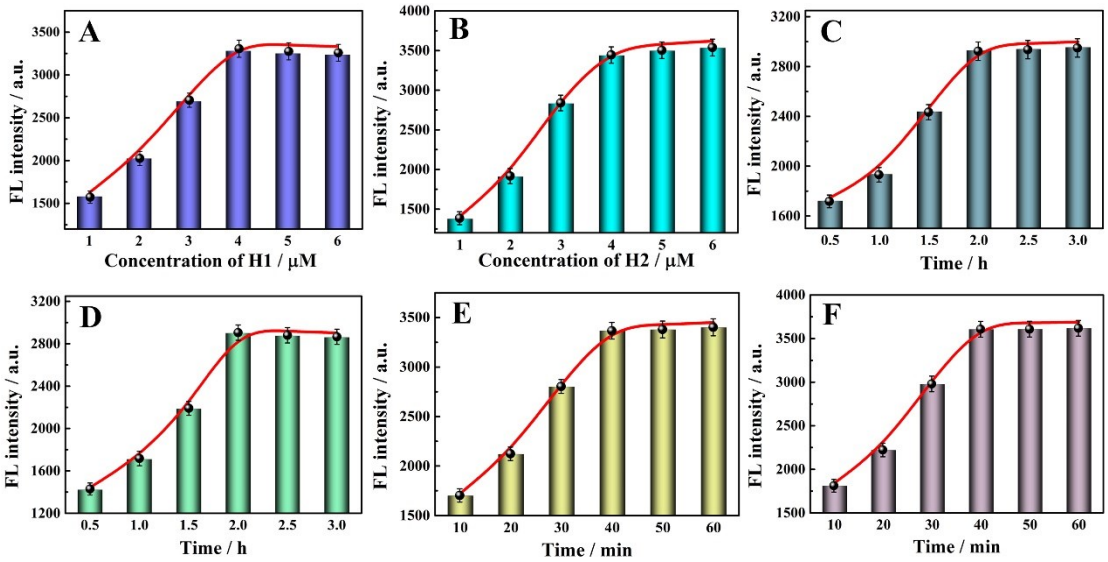

Fig. S7. Relationship between the fluorescent intensity and (A, B) the concentration of H1 and H2, (C, D) the incubation time of the miRNA-21 and miRNA-155 for exporting the double feet catalyst strands A and B, (E, F) fluorescence recovery time of the fluorophore FAM and Cy5.

Application of the Janus 3D DNA Nanomachine in Simultaneous and Sensitive Detection

The application performances of this proposed fluorescence assay based on the dual-color fluorescent Janus nanoparticles was investigated by simultaneously

quantitative determination of miRNA-21 and miRNA-155 with various concentrations in the range from 1 pM to 10 nM. Firstly, the fluorescence responses of the proposed Janus 3D DNA nanostructure for diverse concentrations of miRNA 21 and miRNA-155 were performed in **Fig. S8A** and **S8C**. The fluorescent intensity gradually increased with the concentrations of miRNA-21 and miRNA-155, suggesting that the concentration of target miRNA-21 and miRNA-155 and the fluorescent signal intensity existed in a significant dose-response relationship, which was the basis of quantitative analysis and detection. Furthermore, the relationship between the fluorescence emissions and the concentrations of miRNA-21 and miRNA-155 could be demonstrated as $I = 917.24 \lg c_{\text{miRNA-21}} + 1223.65$ and $I = 918.84 \lg c_{\text{miRNA-155}} + 1026.42$ with the correlation coefficient of $r = 0.998$ and $r = 0.998$, in which I represented the fluorescent intensity and $c_{\text{miRNA-21}}$ and $c_{\text{miRNA-155}}$ were the concentration of miRNA-21 and miRNA-155, respectively (**Fig. S8B** and **S8D**). Simultaneously, the limit of detection (LOD) were determined to be 0.35 pM for miRNA-21 and 0.48 pM for miRNA-155 on the basis of the standard 3σ rule. These results demonstrated that the proposed Janus nanoparticles as carrier immobilized two different DNA substrates on two different functionalized hemispheres of the one nanoparticle are applicable in simultaneous detection of dual miRNAs and hold potential in highly sensitive biomedical detection and metrology.

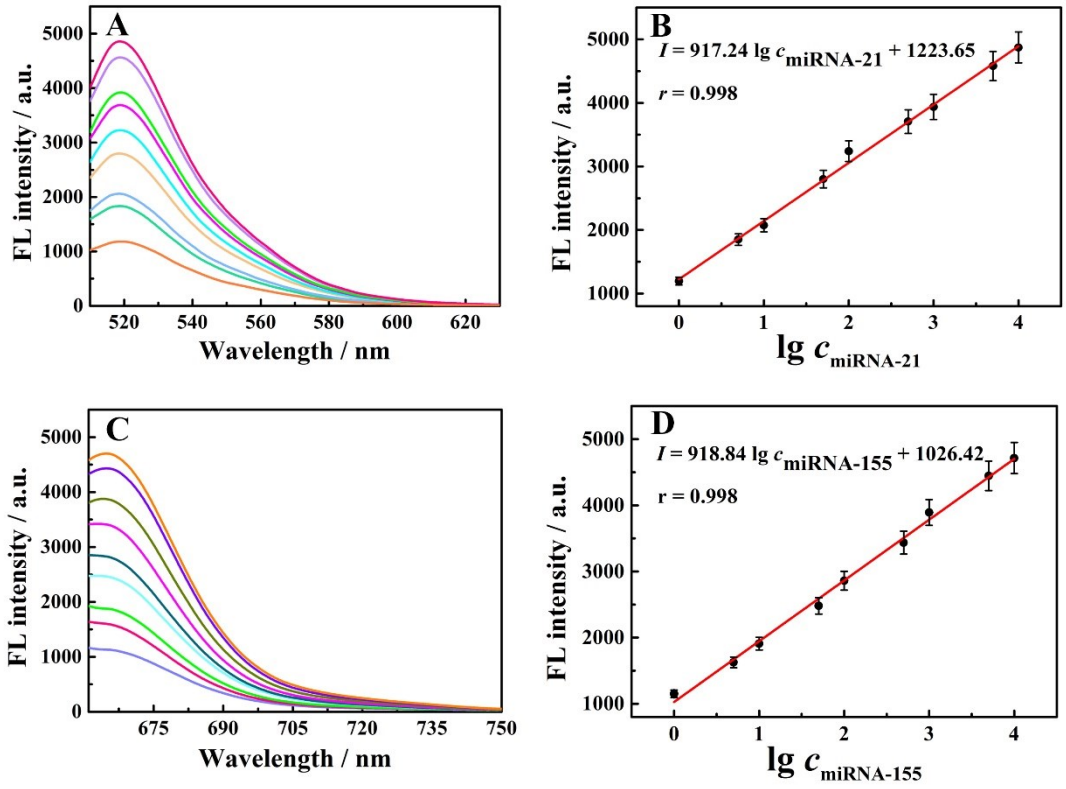

Fig. S8. (A, C) The fluorescence emission spectra of the detection solutions with different miRNA-21 and miRNA-155 concentrations (1 pM, 5 pM, 10 pM, 50 pM, 100 pM, 500 pM, 1 nM, 5 nM, and 10 nM). (B, D) Calibration curve of the fluorescence intensity and the logarithmic concentration of target miRNA-21 and miRNA-155, respectively.

It is critical that signal change is related with the target concentration, which is the basis of quantitative analysis, performing in the linear response interval, slope, etc. In fluorescence detection system, the linear response slope and limit of detection (LOD) is a very important factor, which reflected the amplification efficiency of the detection system. Furthermore, the amplification efficiency results from the contrast of with amplification and without amplification. Therefore, amplification efficiency of the proposed system was investigated using no amplification strategy as control (**Fig. S9**).

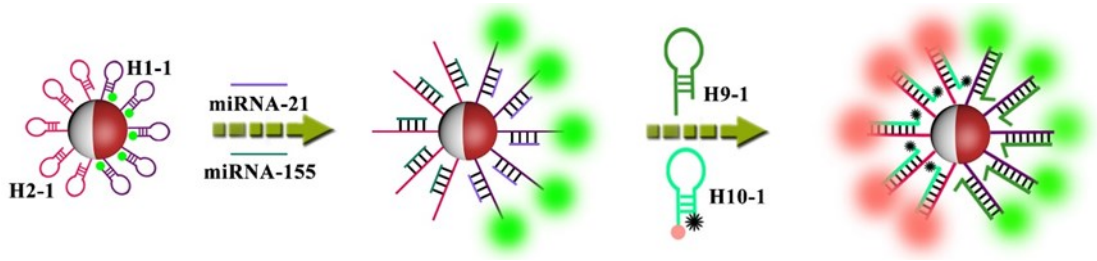

Fig. S9. Schematic illustration of the fluorescent assay based on Janus 3D DNA nanostructure without amplification strategy as control for simultaneous detection of miRNA-21 and miRNA-155.

The carboxyl-labeled H2-1 and FAM and sulfydryl-labeled H1-1 were respectively immobilized on the two different hemispheres of Janus nanoparticles to construct Janus 3D DNA nanostructure. In the presence of miRNA-21, miRNA-155, H9-1 and H10-1, the fluorescence of FAM and Cy5 was recovered. As shown **Fig. S10A** and **S10B**, two linear calibration curves were obtained by plotting the fluorescence intensities versus the logarithmic concentrations of the miRNA-21 and the miRNA-155 with various concentrations (100 pM, 250 pM, 500 pM, 1 nM, 2.5 nM, 5 nM, 10 nM), respectively. The relationship between the fluorescence emissions and the concentrations of miRNA-21 and miRNA-155 could be demonstrated as $I = 766.08 \lg c_{\text{miRNA-21}} - 145.99$ and $I = 770.25 \lg c_{\text{miRNA-155}} - 127.19$ with the correlation coefficient of $r = 0.998$ and $r = 0.998$, in which I represented the fluorescent intensity and $c_{\text{miRNA-21}}$ and $c_{\text{miRNA-155}}$ were the concentration of miRNA-21 and miRNA-155, respectively. The LOD was determined to be 38 pM for miRNA-21 and 51 pM for miRNA-155 on the basis of the standard 3σ rule. Comparison with no amplification strategy, the proposed Janus 3D DNA nanomachine based on cascade signal amplification strategy revealed LOD as low as 100 times and higher linear response slope. These results demonstrated that our detection system possessed high amplification efficiency for sensitive detection of miRNA-21 and miRNA-155.

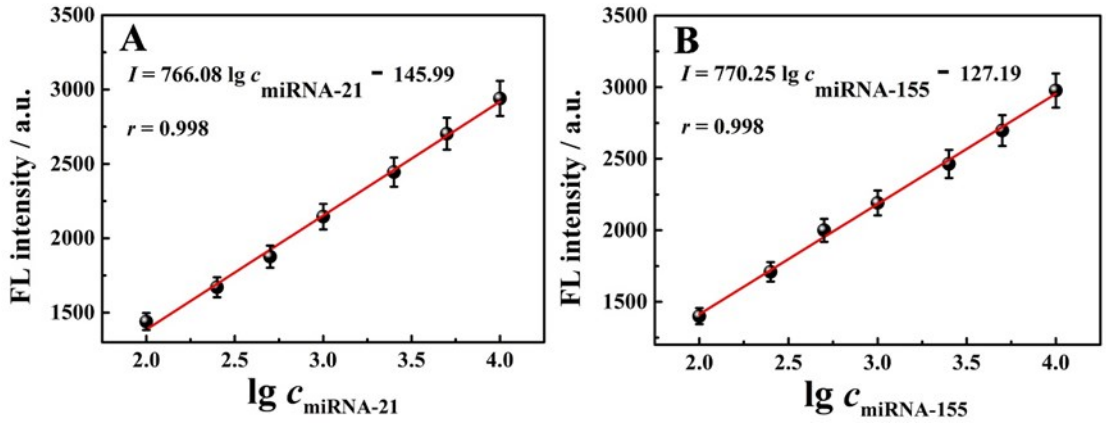

Fig. S10. (A and B) Calibration curve of the fluorescence intensity and the logarithmic concentration of target miRNA-21 and miRNA-155 in the absence of amplification strategy as control, respectively.

Table S2. Nucleic acid sequences used in control experiment

Names	Sequences (5'-3')
H1-1	SH-TCA ACA TCA GTC TGA TAA GCA TGT ATG TAA TGT GTG TAG ATT ATC AGA CT-FAM
H2-1	COOH-TTT TTT TTT TAC CCC TAT CAC GAT TAG CAT TAA GAT CCC GGT ATG CAT TCT AAT CGT GAT A
H9-1	AGT CTG ATA ATC TAC ACA CAT TAC ATA CAT GCT TAT CAG ACT GAT GTG TAG ATT AT
H10-1	Cy5-TAT CAC GAT TAG AAT GCA TAC CGG GAT CTT AAT GCT AAT CGT GAT AGG GGT ATG CAT TCT AAT C-BHQ

Simultaneous and Sensitive Imaging of miRNAs in Living Cells

To estimate the feasibility of the Janus 3D DNA nanomachine for simultaneous and sensitive fluorescent imaging of the intracellular miRNAs, the H1 modified Au@SiO_2-NH_2 NPs, the H2 modified SiO_2-NH_2 NPs and corresponding DNA

substrates as control experiments were delivered into MCF-7 cells with relatively high expression of miRNA-21 and miRNA-155. After incubating different nanoparticles and corresponding DNA substrates and different FISH probes with MCF-7 cells, the significantly discrepant fluorescence signal could be observed (**Fig. S11**). As expected, when the H1 modified Au@SiO_2-NH_2 NPs were delivered into MCF-7 cells, it exhibited apparent fluorescence responses of the FAM (**Fig. S11A**). However, FAM-labeled FISH probes incubated with MCF-7 cells, only very weak green fluorescence could be observed (**Fig. S11B**). In the presence of the H2 modified SiO_2-NH_2 NPs, the conspicuous fluorescence of Cy5 could be observed (**Fig. S11C**). However, when the Cy5-labeled FISH probes were delivered into MCF-7 cells, only very weak red fluorescence could be observed (**Fig. S11D**). The results of these control experiments indicate that the proposed Janus 3D DNA nanomachine could be used for sensitive imaging of dual miRNAs in cells.

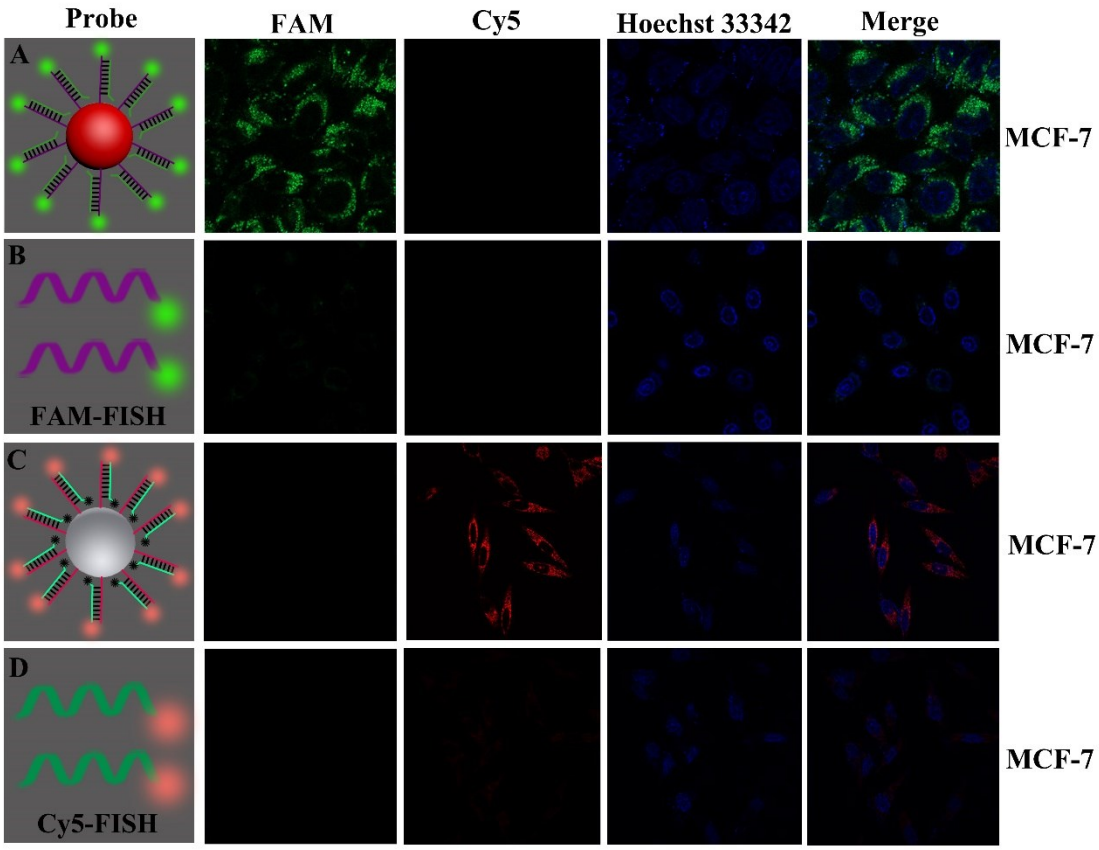

Fig. S11. CLSM images of miRNA-21 and miRNA-155 in MCF-7 cells obtained with Au@SiO_2-NH_2 NPs and SiO_2-NH_2 NPs-based fluorescent method (A, C) and the conventional FISH method (B, D). The cell nucleus are shown in blue, and the fluorophore FAM and Cy5 corresponding to the miRNA-21 and the miRNA-155 are in green and red, respectively.

Further verification of the Janus 3D DNA nanomachine for simultaneous and sensitive imaging of dual miRNAs in the cancer cells, the H1 modified Au@SiO_2-NH_2 NPs, the H2 modified SiO_2-NH_2 NPs, corresponding DNA substrates and different FISH probes were delivered into HeLa cells with relatively low concentration of miRNA-21 and highly overexpressed level of miRNA-155, respectively. As shown in **Fig. S12**, after incubating H1 modified Au@SiO_2-NH_2 NPs with HeLa cells, only very weak fluorescence of FAM could be observed (**Fig. S12A**), indicating lowly expressed intracellular miRNA-21 in HeLa cells. At the same time, FAM-labeled FISH probes

incubated with HeLa cells, no fluorescence signal distinguished from the background was observed, which indicated that the relative low expression levels of miRNA-21 in HeLa cells was failed to be detected by the traditional FISH approach (**Fig. S12B**). When the H2 modified SiO_2-NH_2 NPs were transferred into cells, the fluorescence of Cy5 was extraordinarily strong (**Fig. S12C**), which suggested that the miRNA-155 was highly overexpressed in HeLa cells. However, Cy5-labeled FISH probes incubated with HeLa cells, only very weak red fluorescence could be observed (**Fig. S12D**). These results further demonstrated the proposed Janus 3D DNA nanomachine could not only sensitively image highly overexpressed miRNAs, but also make it possible to visualize extraordinarily low concentration of miRNAs in cancer cells with high accuracy over conventional FISH method.

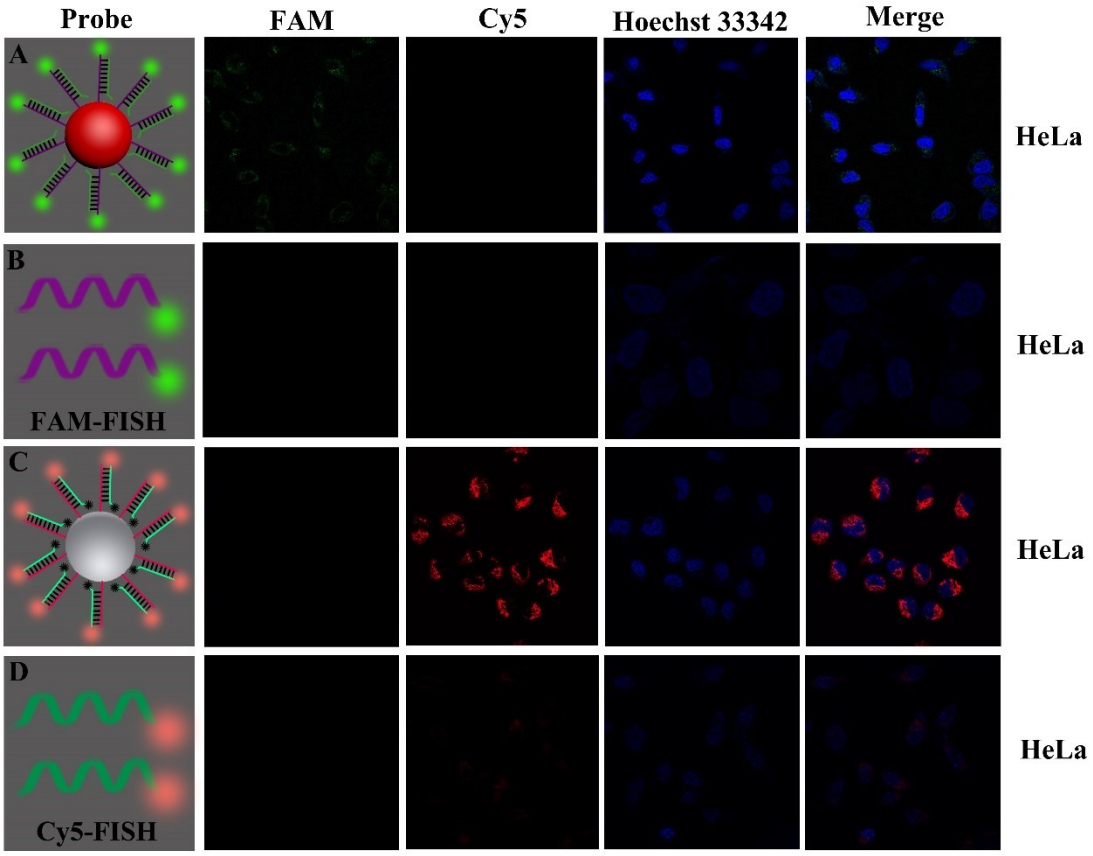

Fig. S12. CLSM images of miRNA-21 and miRNA-155 in HeLa cells obtained with Au@SiO_2-NH_2

NPs and SiO_2-NH_2 NPs-based fluorescent method (A, C) and the conventional FISH method (B, D). The cell nucleus are shown in blue, and the fluorophore FAM and Cy5 corresponding to the miRNA-21 and the miRNA-155 are in green and red, respectively.

Selectivity of the Proposed Strategy for Simultaneous Detection of miRNA-21 and miRNA-155

To evaluate the specificity of our proposed fluorescent assay for simultaneous detection of miRNA-21 and miRNA-155, a series of commonly coexisting miRNAs, containing miRNA-122, miRNA-126, miRNA-141, miRNA-203a and miRNA-182-5p have been selected as controlling factors. The experimental results shown in **Fig. S13**, a low fluorescence intensity was observed when the sample was only these interfering miRNAs, and the fluorescence intensity was close to the blank sample, even though the concentration of potential interfering substances was 100 times higher than miRNA-21 and miRNA-155. However, even the target miRNA-21 and miRNA-155 with 500 pM, the fluorescence intensity was apparently increased. In the meantime, for the mixture of the miRNA-21 and miRNA-155 with the interfering miRNAs, the fluorescence intensity was almost consistent with miRNA-21 and miRNA-155. These results sequentially indicated that the proposed fluorescent assay possesses excellent selectivity for simultaneous detection of miRNA-21 and miRNA-155.

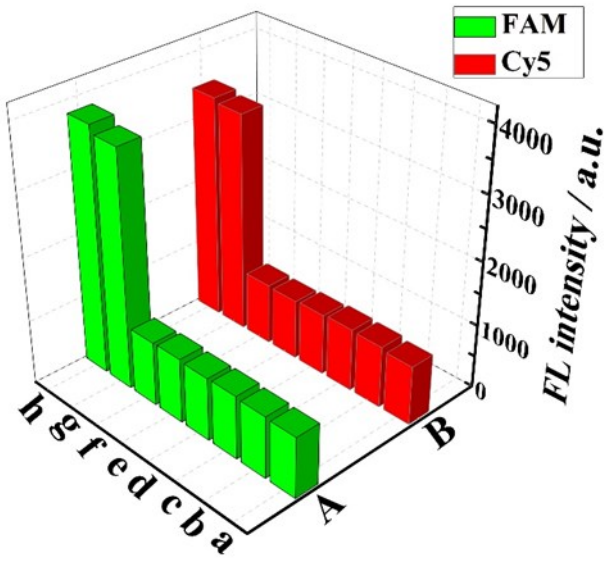

Fig. S13. Specificity of the proposed strategy toward miRNA-21 (A) and miRNA-155 (B): (a) blank sample, (b) miRNA-122 (50 nM), (c) miRNA-126 (50 nM), (d) miRNA-141 (50 nM), (e) miRNA-203a (50 nM), (f) miRNA-182-5p (50 nM), (g) miRNA-21 (500 pM) and miRNA-155 (500 pM), (h) mixed sample.

To further evaluate the specificity of our proposed fluorescent assay for simultaneous detection of miRNA-21 and miRNA-155, a series of mismatched sequences of the targets miRNA-21 and miRNA-155, containing single-base mismatch, double-base mismatch and triple-base mismatch have been selected as controlling factors. As shown in **Fig. S14A**, a low fluorescence intensity was observed when the sample was only these mismatched sequences of the target miRNA-21 (**Fig. S14A**, parts b, b1, c, c1, d, d1, e, e1, f and f1), and the fluorescence intensity was approximate to the blank sample (**Fig. S14A**, part a), even though the concentration of these mismatched sequences was 100 times higher than target miRNA-21. On the contrary, in the presence of miRNA-21 with 500 pM (**Fig. S14A**, part g), the fluorescence intensity was remarkably increased. Simultaneously, for the mixture of miRNA-21 with

these mismatched sequences (**Fig. S14A**, part h), the fluorescence intensity was almost consistent with miRNA-21 only. As shown in **Fig. S14B**, in the presence of these mismatched sequences of the target miRNA-155 (**Fig. S14B**, parts B, B1, C, C1, D, D1, E, E1, F and F1), a low fluorescence intensity was observed, which was approximate to that of the blank sample (**Fig. S14B**, part A), even though the concentration of these mismatched sequences was 100 times higher than miRNA-155. However, even the target miRNA-155 with 500 pM (**Fig. S14B**, part G), the fluorescence intensity was conspicuously increased. In the meantime, for the mixture of the miRNA-155 with these mismatched sequences of the target miRNA-155 (**Fig. S14B**, part H), the fluorescence intensity was almost consistent with miRNA-155 only. These results furtherly demonstrated that the proposed fluorescent assay possessed excellent specificity for simultaneous detection of miRNA-21 and miRNA-155 in the presence of these mismatched sequences of the target miRNA-21 and miRNA-155.

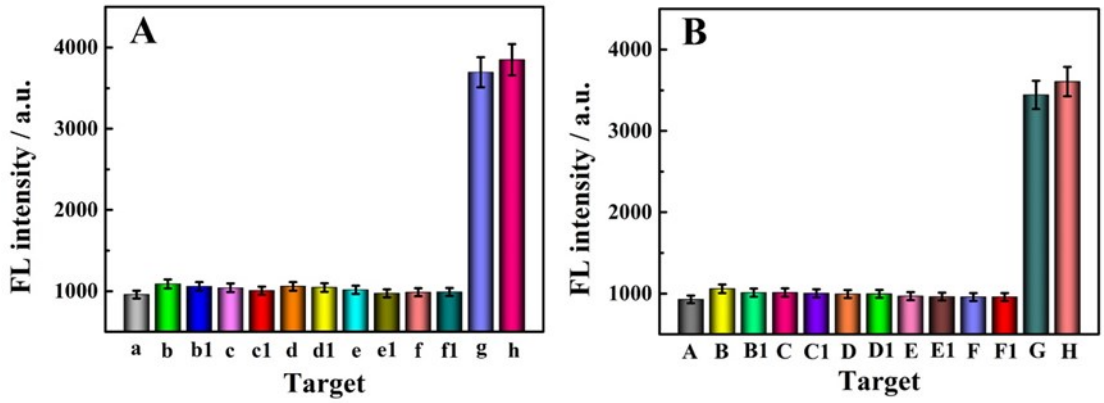

Fig. S14. (A) Specificity of the proposed strategy toward miRNA-21. (a) blank sample, (b) miRNA-21-b (50 nM), (b1) miRNA-21-b1 (50 nM), (c) miRNA-21-c (50 nM), (c1) miRNA-21-c1 (50 nM), (d) miRNA-21-d (50 nM), (d1) miRNA-21-d1 (50 nM), (e) miRNA-21-e (50 nM), (e1) miRNA-21-e1 (50 nM), (f) miRNA-21-f (50 nM), (f1) miRNA-21-f1 (50 nM), (g) miRNA-21 (500 pM), (h)

mix sample. (B) Specificity of the proposed strategy toward miRNA-155. (A) blank sample, (B) miRNA-155-B (50 nM), (B1) miRNA-155-B1 (50 nM), (C) miRNA-155-C (50 nM), (C1) miRNA-155-C1 (50 nM), (D) miRNA-155-D (50 nM), (D1) miRNA-155-D1 (50 nM), (E) miRNA-155-E (50 nM), (E1) miRNA-155-E1 (50 nM), (F) miRNA-155-F (50 nM), (F1) miRNA-155-F1 (50 nM), (G) miRNA-155 (500 pM), (H) mix sample.

Table S3. Mismatched sequence of the target miRNA-21 and miRNA-155

Names	Sequences (5'-3')
miRNA-21-b	UAG CUU AUG AGA CUG AUG UUG A
miRNA-21-b1	UAG CUU AUC AGA CUG AUG UUU A
miRNA-21-c	UAG CGG AUC AGA CUG AUG UUG A
miRNA-21-c1	UAG CUU AUC AGA CUG GCG UUG A
miRNA-21-d	UAG CUU UUC AGU CUG AUG UUG A
miRNA-21-d1	UAG CUU AUC AGA CGG AUG AUG A
miRNA-21-e	UAG CUU AUC UUC CUG AUG UUG A
miRNA-21-e1	UAG CUU AUC AGA CUG AUG GGA A
miRNA-21-f	UAG AUU AGC AGG CUG AUG UUG A
miRNA-21-f1	UAG CUU AUC CGA CCG AUU UUG A
miRNA-155-B	UUA AUG CUG AUC GUG AUA GGG GU
miRNA-155-B1	UUA AUG CUA AUC GUG AGA GGG GU
miRNA-155-C	UUA AUG CUA AGU GUG AUA GGG GU
miRNA-155-C1	UUA AUG CUA AUC GUG AUA UUG GU
miRNA-155-D	UUA AGG CUA CUC GUG AUA GGG GU
miRNA-155-D1	UUA AUG CUA AUC UUG AUC GGG GU
miRNA-155-E	UUA AUG CUA AUC UCU AUA GGG GU
miRNA-155-E1	UUA AUG CUA AUC GUG AUA GUU AU
miRNA-155-F	UUG AUG UUA AGC GUG AUA GGG GU
miRNA-155-F1	UUA AUG CUA AUU GUG GUA GUG GU

CLSM Imaging with Different Depth of the Z-axis in Living Cancer Cells

In order to obtain intuitionistic images of the intracellular dual miRNAs in MCF-7 cells and HeLa cells, the CLSM images were performed. As shown in **Fig. S15A** to **Fig. S15F**, the fluorophore FAM of green (FAM for the miRNA-21) and the fluorophore Cy5 of red (Cy5 for the miRNA-155) were respectively observed in MCF-7 cells on different depth of the Z-axis with excitation at 488 nm and 640 nm, indicating relatively high expression levels of miRNA-21 and miRNA-155 in MCF-7 cells. As shown in **Fig. S15H** to **Fig. S15M**, although the fluorescence intensity of the side labeled the fluorophore Cy5 was significantly stronger than that of the side labeled the fluorophore FAM in HeLa cells, the fluorescence of green could be still observed. These results clearly revealed the practical capability of Janus 3D DNA nanomachine for sensitive imaging of two intracellular miRNAs.

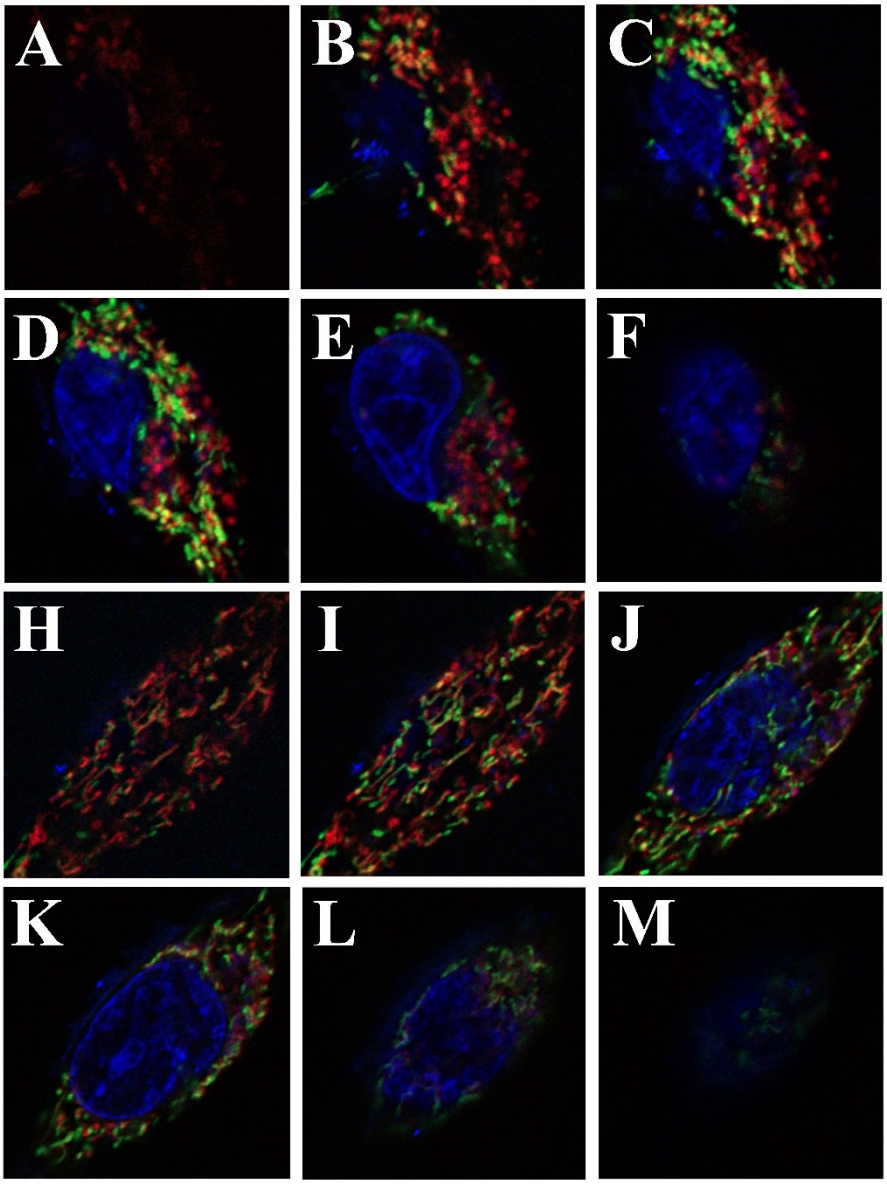

Fig. S15. CLSM imaging of the Janus 3D DNA nanomachine in MCF-7 cells (A-F) and HeLa cells (H-M) with excitation at 488 nm and 640 nm on different depth of the Z-axis.

Detection of Cells Lysates

In order to evaluate practical application capability of the proposed strategy for the simultaneous determination of intracellular miRNA-21 and miRNA-155, real samples from different cell lines were employed for the *in vitro* measurements, including the MCF-7 cells with highly overexpressed level of miRNA-21 and miRNA-

155 and HeLa cells with low expression of miRNA-21 and high expression of miRNA-155. As presented in **Fig. S16A**, with the number of MCF-7 cells increasing from 1 × 10^3 to 100 × 10^5, the fluorescence intensity distinctly increased for detection of miRNA-21 and miRNA-155. These results suggested that the miRNA-21 and miRNA-155 was highly overexpressed in MCF-7 cells, which has been previously demonstrated by researches.[5-7] As shown in **Fig. S16B**, the fluorescence intensity of the lysates extracted from HeLa cells has a low fluorescence response and slow growth for miRNA-21 detection. On the country, with the increasing number of HeLa cells from 1 × 10^3 to 100 × 10^5, the fluorescence intensity obviously increased for miRNA-155. At the same time, the fluorescence intensity of miRNA-155 detection was conspicuously higher than miRNA-21 detection, indicating that the expression level of miRNA-155 is much higher than miRNA-21 in HeLa cells. These results indicated that the proposed Janus 3D DNA nanomachine could be employed to simultaneously distinguish the different expression levels of miRNAs in the cancer cells.

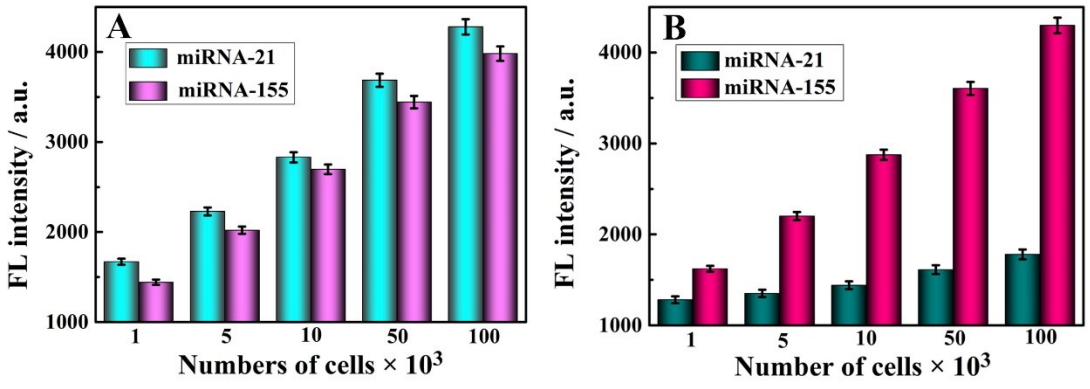

Fig. S16. Practical application of the proposed Janus 3D DNA nanomachine for simultaneous detection of miRNA-21 and miRNA-155 in diverse cancer-cell lysates between MCF-7(A) and HeLa cells (B).

Table S4. Comparison of the developed Janus 3D DNA nanomachine with other miRNA detection methods

Target	Detection method	Limit of Detection	Linear range	Ref.
miRNA-21	Photoacoustic Imaging	11.69 pM	10 pM-100 nM	8
miRNA-21	Electrochemistry	40 pM	0.14 nM-10 nM	9
miRNA-21	Fluorescence	33 pM	0.1 nM-4 nM	10
miRNA-21	Fluorescence	47 pM	0.15 nM-16 nM	11
miRNA-21	Fluorescence	0.35 pM	1 pM-10 nM	***This work***
miRNA-155	Electrochemical	5.2 pM	0.01 nM to 1000 nM	12
miRNA-155	Fluorescence	85.3 pM	100 pM to 50 nM	13
miRNA-155	Fluorescence	680 pM	1 nM to 100 nM	14
miRNA-155	Fluorescence	0.48 pM	1 pM-10 nM	***This work***

Supplementary References

1. J. J. Peng, J. Y. Li, W. Xu, L. Wang, D. D. Su, C. L. Teoh and Y. T. Chang, *Anal. Chem.*, 2018, **90**, 1628-1634.
2. M. E. Hafez, H. Ma, W. Ma and Y. T. Long, *Angew. Chem. Int. Ed.*, 2019, **131**, 6393-6398.
3. Y. Y. Li, W. G. Alex, M. S. Daniel, X. L. Yang, Z. C. Yu, Y. N. Tang and F. Li, *Chem. Sci.*, 2018, **9**, 6434-6439.
4. C. Jung, P. B. Allen and A. D. Ellington, *ACS Nano*, 2017, **11**, 8047-8054.
5. S. Volinia, G. A. Calin, C. G. Liu, S. Ambs, A. Cimmino, F. Petrocca, R. Visone, M. Iorio, C. Roldo, M. Ferracin, R. L. Prueitt, N. Yanaihara, G. Lanza, A. Scarpa, A. Vecchione, M. Negrini, C. C. Harris and C. M. Croce, *Proc. Natl. Acad. Sci. U. S. A*., 2006, **103**, 2257-2261.
6. S. Hu, W. Zhu, L. F. Zhang, M. Pei and M. F. Liu, *Cell Res*., 2014, **24**, 254-257.
7. Y. Cao, S. Z. Li, C. Chen, D. D. Wang, T. T. Wu, H. F. Dong and X. J. Zhang, *Biomaterials*, 2018, **158**, 23-33.
8. K. Zhang, X. D. Meng, Z. Yang, Y. Cao, Y. R. Cheng, D. D. Wang, H. T. Lu, Z. J. Shi, H. F. Dong and X. J. Zhang, *Adv. Mater.*, 2019, **31**, 1807888.
9. S. Campuzano, R. M. Torrente-Rodriguez, E. Lopez-Hernandez, F. Conzuelo, R. Granados, J. M. Sanchez-Puelles and J. M. Pingarron, *Angew. Chem. Int. Ed.*, 2014, **53**, 6168-6171.
10. H. M. Fang, N. L. Xie, M. Ou, J. Huang, W. S. Li, Q. Wang, J. B. Liu, X. H. Yang and K. M. Wang, *Anal. Chem.*, 2018, **90**, 7164-7170.

11. S. J. Zhen, X. Xiao, C. H. Li and C. Z. Huang, *Anal. Chem*., 2017, **89**, 8766-8771.

12. D. Q. Kong, S. Bi, Z. H. Wang, J. F. Xia and F. F. Zhang, *Anal. Chem.*, 2016, **88**, 10667-10674.

13. F. Yang, Y. R. Cheng, Y. Cao, Y. Y. Zhang, H. F. Dong, H. T. Lu and X. J. Zhang, *Anal. Chem.*, 2019, **91**, 9828-9835.

14. F. Yang, Y. R. Cheng, Y. Cao, H. F. Dong, H. T. Lu, K. Zhang, X. D. Meng, C. H. Liu and X. J. Zhang, *Chem. Sci.*, 2019, **10**, 1709-1715.